# Rill erosion in natural and disturbed forests: 2. Modeling Approaches

J. W. Wagenbrenner,[1] P. R. Robichaud,[1] and W. J. Elliot[1]

Received 19 June 2009; revised 30 March 2010; accepted 19 April 2010; published 8 October 2010.

[1] As forest management scenarios become more complex, the ability to more accurately predict erosion from those scenarios becomes more important. In this second part of a two-part study we report model parameters based on 66 simulated runoff experiments in two disturbed forests in the northwestern U.S. The 5 disturbance classes were natural, 10-month old and 2-week old low soil burn severity, high soil burn severity, and logging skid trails. In these environments the erosion rates were clearly detachment limited, and the rill erodibility parameters calculated from four hydraulic variables increased by orders of magnitude. The soil shear stress based erodibility parameter, $K_r$, was $1.5 \times 10^{-6}$ s m$^{-1}$in the natural plots, $2.0 \times 10^{-4}$ s m$^{-1}$ in the high soil burn severity plots, and $1.7 \times 10^{-3}$ s m$^{-1}$ in the skid trail plots; $K_r$ values for the low soil burn severity plots had negative sign. The erodibility value for the skid trail plots fell within ranges reported for tilled agricultural fields and also for forest roads. The $K_r$ values decreased as erosion occurred in the plots and therefore should not be a constant parameter. The stream power produced the largest $R^2$ value (0.41) when hydraulic predictors and the sediment flux were log-transformed, but none of the four hydraulic variables (soil shear stress, stream power, unit stream power, and unit length shear force) explained much of the variability in sediment flux rates across the five levels of disturbance when evaluated in the linear form of the erosion models under consideration.

**Citation:** Wagenbrenner, J. W., P. R. Robichaud, and W. J. Elliot (2010), Rill erosion in natural and disturbed forests: 2. Modeling Approaches, *Water Resour. Res.*, *46*, W10507, doi:10.1029/2009WR008315.

## 1. Introduction

[2] In the western United States, forestry management decisions affect a large portion of public lands and many different uses and activities. When assessing the environmental impacts of various decisions, potential soil loss through erosion is an important consideration. Since empirical erosion data are scarce and time- and cost-intensive to collect, managers often depend on erosion models to make these assessments. To be fully effective these models must be designed for various management scenarios and diverse environments. Most of the currently available erosion models used for forest environments evolved from models that were developed from plot studies on agricultural soils with low slopes [*Bryan*, 2000]. Experiments in forest environments where soils are shallow and slopes are steep are necessary if erosion models are to be usable for forest conditions.

[3] Most physically based water erosion models divide erosion into inter-rill or splash and sheet flow erosion, and rill or concentrated flow erosion [*Foster and Meyer*, 1972; *Foster*, 1982]. Sediment delivery may be limited either by the ability of the erosive agents to detach the sediment (detachment or source limited), or by the ability of the runoff to transport the sediment (transport limited) [*Ellison*, 1946; *Foster and Meyer*, 1972; *Foster*, 1982]. As concentrated flow further increases in amount or duration, channel processes such as bed and bank scour and sediment transport begin to dominate sediment movement [*Hairsine and Rose*, 1992b]. The study described in this paper is aimed at better understanding and modeling the upland rill erosion processes on steep disturbed forested hillslopes.

[4] Early modeling efforts focused on transport capacity, detachment capacity, and flow mechanics such as hydraulic shear stress and stream power as drivers for erosion. *Foster and Meyer* [1972] proposed a rill and inter-rill erosion model where the rill erosion component of that model was a function of hydraulic shear stress. This approach was subsequently incorporated into the Water Erosion Prediction Project (WEPP) model [*Nearing et al.*, 1989].

[5] The erosion component of the WEPP model [*Nearing et al.*, 1989] was one of the first physically based models to account for soil erosion and sediment transport from both inter-rill and rill areas, and is described by

$$\frac{dG}{dx} = D_r + D_i \tag{1}$$

where $x$ is the distance down the slope (m), $G$ is the sediment load per unit width (kg s$^{-1}$ m$^{-1}$), $D_r$ is the rill erosion rate (kg s$^{-1}$ m$^{-2}$) and $D_i$ is the inter-rill erosion rate (kg s$^{-1}$ m$^{-2}$).

[6] The erosion from inter-rill areas, $D_i$, is calculated using an inter-rill erodibility parameter, $K_i$ (kg s$^{-1}$ m$^{-4}$), and

[1]Forestry Sciences Laboratory, Rocky Mountain Research Station, Forest Service, U.S. Department of Agriculture, Moscow, Idaho, USA.

is a function of rainfall intensity and runoff rate. The rill sediment detachment capacity, $D_c$ (kg s$^{-1}$ m$^{-2}$), is the amount of soil that can be dislodged by the water per unit area and time and is a product of the rill erodibility parameter, $K_r$ (s m$^{-1}$), which is a soil property, and the excess soil shear stress, $\tau_s$ (kg s$^{-2}$ m$^{-1}$ or Pa). Some stress must be applied to the soil before detachment occurs, and this has been termed the critical shear stress, $\tau_c$ (kg s$^{-2}$ m$^{-1}$), leading to an equation in the form of [*Foster et al.*, 1995]

$$D_c = K_r(\tau_s - \tau_c) \tag{2}$$

[7] *Foster and Meyer* [1972] noted in field observations that as the amount of sediment in transport increases, the detachment decreases. They proposed a model to describe this process as

$$\frac{D_r}{D_c} + \frac{q_s}{T_c} = 1 \tag{3}$$

where $q_s$ is the sediment flux rate (kg s$^{-1}$) and $T_c$ is the sediment transport capacity of clear water (kg s$^{-1}$). If the detachment rate is assumed to be the differential of $G$ (equation (1)), equation (3) becomes [*Elliot et al.*, 1989]

$$\frac{dG(x)}{dx} = D_c(x)\left[1 - \frac{q_s(x)}{T_c(x)}\right] \tag{4}$$

[8] The above equations demonstrate how *Foster and Meyer* [1972] assumed that once sediment was entrained in the rill flow, the sediment was either delivered to the outlet of the rill or, when the rill sediment flux equaled the flow's sediment transport capacity, it was deposited in the rill. When the sediment in transport exceeded the transport capacity, sediment deposition would begin as a function of particle fall velocity, with larger sand particles depositing first and smaller or less dense aggregates and clay particles depositing last. The transport limiting condition may occur in agricultural settings due to relatively high availability of detachable soil particles and relatively low transport capacities achieved on low slopes. The transport capacity in mountainous forests often is much greater than the values reported for agricultural settings [*Elliot et al.*, 1989; *Hairsine and Rose*, 1992a, 1992b; *McIsaac et al.*, 1992; *Giménez and Govers*, 2002]. *Foster* [1982] indicated that if the sediment flux rate was less than the flow's transport capacity, additional detachment would occur in the rill to either 1) achieve the transport capacity, or 2) achieve the rill detachment capacity.

[9] *Hairsine and Rose* [1992a, 1992b] also developed a rill erosion model that results in less sediment detachment as the amount of sediment in transport increases. In their model, sediment entrainment and deposition can occur simultaneously [*Hairsine and Rose*, 1992a, 1992b]. In rill segments where the sediment flux rate is low, the deposition also will be low so the dominant process will be detachment of cohesive soil from the sides and bottoms of the rill. In rill segments where the sediment flux rate is high, deposition will become more pronounced, and the entrainment process will be dominated by entrainment of non-cohesive sediment—sediment that had been previously detached and subsequently deposited—from the rill bottom, with some detachment of cohesive sediment from the rill sides. Based on these *assumptions*, *Hairsine and Rose* [1992b] developed a stream power rill erosion model with the form

$$Q\frac{dc_i}{dx} + c_i\frac{dQ}{dx} = [(1-H)W_b + W_s]\left[\frac{F(\Omega - \Omega_0)}{IJ}\right] + q_{syi} \tag{5}$$

where $Q$ is the volumetric flow rate per rill (m$^3$ s$^{-1}$), $c_i$ is the sediment concentration of particle size class $i$ (kg m$^{-3}$), $H$ is the fraction of the rill wetted perimeter base covered by deposited sediment, $W_b$ is the width of the base of a trapezoidal rill (m), $W_s$ is the horizontal width of the sides of a trapezoidal rill (m), $F$ is the fraction of excess stream power ($\Omega - \Omega_0$) used in entraining or re-entraining sediment in class size $i$, $\Omega_0$ is the stream power below which no entrainment occurs (kg s$^{-3}$), $I$ is the number of settling velocity classes, $J$ is the specific energy of entrainment (J kg$^{-1}$ or m$^2$ s$^{-2}$), and $q_{syi}$ is the inter-rill contribution to sediment in the rill (kg s$^{-1}$ m$^{-1}$). *Hairsine and Rose* [1992b] concluded that the $J$ term can only be derived from erosion experiments, suggesting it may be related to fall cone or shear device measurements. Other researchers, however, did not find field- or lab-measured soil strength properties useful for predicting rill soil erodibility [*Elliot et al.*, 1990].

[10] The work of *Hairsine and Rose* [1992a, 1992b] has been supported by more recent studies that found stream power to be a better predictor of rill detachment rates than shear stress [*Elliot and Laflen*, 1993; *Nearing et al.*, 1997; *Pannkuk and Robichaud*, 2003]. *Bryan* [2000] suggested that different erosion predictors work better for different experimental designs. In an extensive laboratory and field study on agricultural soils, stream power was found to be the best predictor of unit sediment load (sediment per unit time per unit width) [*Nearing et al.*, 1997]. *Nearing et al.* [1999] found that sediment detachment rates were better correlated in a power function of either shear stress ($R^2$ = 0.51) or stream power ($R^2$ = 0.59) than in a linear function of shear stress. In a laboratory study on burned soils, stream power was shown to be a better predictor of rill erosion than shear stress ($R^2$ = 0.56 and 0.24, respectively) [*Pannkuk and Robichaud*, 2003].

[11] The unit stream power, $\Omega_u$ (m s$^{-1}$), has also been shown to effectively predict rill erosion rates [*McIsaac et al.*, 1992; *Morgan et al.*, 1998]. The unit stream power rill erosion model takes the form

$$q_s = K_{\Omega_u}(\Omega_u - \Omega_{u0}) \tag{6}$$

where $q_s$ is the sediment flux rate (kg s$^{-1}$), $K_{\Omega u}$ is the unit stream power rill erodibility (kg m$^{-1}$) and $\Omega_{u0}$ is the (critical) unit stream power below which no erosion occurs. *McIsaac et al.* [1992] used sediment particle diameter, sediment particle fall velocity, and fluid viscosity to estimate the erodibility term.

[12] *Govers et al.* [2007] presented a critical review of the *Foster and Meyer* [1972] and *Hairsine and Rose* [1992a, 1992b] models as well as a number of similar concentrated flow erosion models that had been proposed in recent decades. They presented data to suggest that soil detachment is not limited by the amount of sediment in transport until the amount of sediment in transport approaches the sediment transport capacity [*Govers et al.*, 2007]. *Giménez and*

*Govers* [2002] suggested a simplified rill erosion model based on the unit length shear force, $\Gamma$ (kg s$^{-2}$)

$$D_L = \alpha\Gamma \quad (7)$$

where $D_L$ is the sediment flux per unit length of rill (kg s$^{-1}$ m$^{-1}$) and $\alpha$ (s m$^{-1}$) is a constant.

[13] Each of these models initially was used to predict erosion from agricultural lands. The WEPP model was intended for use on agricultural, range and forest lands [*Laflen et al.*, 1997]; initial parameterization of the model, however, focused on predicting erosion from heavily disturbed agricultural and range lands [*Elliot et al.*, 1989; *Laflen et al.*, 1991]. Data presented by *Hairsine and Rose* [1992a, 1992b], *McIsaac et al.* [1992], and *Giménez and Govers* [2002] were from either tilled or highly disturbed agricultural soils. *Bryan* [2000] lists some of the limitations of research in agricultural soils, including the homogeneity caused by plowing, changes in soil structure and organic matter content, and lack of macropores. The frequent tillage applied to agricultural plots alters the soil structure, disperses aggregates, increases porosity, and decreases compaction. As a consequence, the tilled layer is more erodible and the rill erodibility would likely be relatively high compared to a forest soil which had never been mechanically disturbed. In comparison, soils in undisturbed forests generally have greater cohesion, a more developed structure, greater aggregate stability, and protection from erosive forces by vegetation, litter, duff, and roots. Forest soils therefore have fewer particles available for detachment unless some disturbance occurs to disrupt this stability.

[14] Recently, use of the WEPP model has expanded into non-agricultural applications, including predictions of erosion from natural and disturbed range and forest hillslopes [*Elliot*, 2004; *Robichaud*, 1996]. Some of the hydrologic [*Robichaud*, 2000] and inter-rill [*Burroughs et al.*, 1992] modeling parameters for forest conditions have been presented but rigorous evaluations of the rill erodibility parameters for forest conditions have not yet been conducted.

[15] The soil parameters in the rill erosion models presented are fixed for all computations once a soil type and disturbance are selected. A recent study on forest roads suggested that rill erosion rates are much higher in the early part of a runoff event than in the latter part of the event [*Foltz et al.*, 2008]. Similarly, *Pierson et al.* [2008] reported changes in sediment concentration during a constant flow, short duration simulated runoff experiment on burned range land. These changes in rill erosion over short time periods may be caused by the winnowing of fine or easily detachable soil particles during the early stages of a runoff event. As the supply of easily erodible particles is smaller in forest soils than in agricultural soils, a constant erodibility model may not apply as well to forest soils as it does to tilled agricultural soils.

[16] In part 1 of this study [*Robichaud et al.*, 2010] we reported differences in runoff rates, runoff velocities, and sediment flux rates among natural forested sites and sites with three types of forest disturbance. The experiment was designed to measure the effects of rill flow on erosion rates, independent of inter-rill flow and sediment contribution. Although this would not occur in any natural system, this control allowed clear identification of the rill erodibility parameters and influences on those parameters. The objectives for the current paper were to 1) determine if the erosion response is detachment-limited or transport-limited; 2) calculate and compare the rill erodibility parameters for five classes of forest disturbance (natural, 10-month old low soil burn severity, 2-week old low soil burn severity, high soil burn severity, and skid trails); 3) determine if the erodibility for a given site changes between initial and late (steady state) runoff periods during a constant inflow; and 4) compare prediction capability among the four hydraulic parameters described above (soil shear stress, stream power, unit stream power and unit length shear force). Implications for erosion modeling are also discussed.

## 2. Methods and Site Description

### 2.1. Site Description

[17] Simulated rill experiments were conducted in two burned forest locations (Tower and North 25). Each location included an area burned by wildfire and a recent timber harvest which was conducted using ground-based skidding equipment. Sites were located in four levels of forest disturbance in each location: natural (recently undisturbed), low soil burn severity (from wildfire), high soil burn severity (from wildfire), and logging skid trails. The experiments were conducted 10 months after the Tower fire and 2 weeks after the North 25 fire, so the two low soil burn severity sites were analyzed as separate disturbance classes while the two high soil burn severity sites were combined in the same class [*Robichaud et al.*, 2010]. Additional characteristics of the sites are shown in Table 1.

### 2.2. Procedure

[18] A series of 5 inflow rates (4, 20, 28, 14, and 45 L min$^{-1}$) were applied to 4-m long rill plots for 12 min each, for a total duration of 60 min. Runoff and sediment samples were collected approximately every 2 min during runoff. Runoff rates, runoff velocities, sediment flux rates, and flow depth and width were measured for each inflow rate. Other details of the site descriptions and experimental procedures may be found in part 1 of this study [*Robichaud et al.*, 2010].

[19] For each inflow rate, all rills 1 m and 3 m from the inflow point were identified and the width, $w$ (m), and depth, $d$ (m), of flow in each rill at each location was measured with a ruler. The hydraulic radius, $R_h$ (m), for each rill and inflow rate was calculated assuming a rectangular cross section. As some of the flow split into multiple rills below the 1 m measurement point, the maximum hydraulic radius from the 1 m and 3 m locations was used in subsequent calculations.

### 2.3. Review of Part 1 Results

[20] The runoff rates, runoff velocities, and sediment flux rates were the lowest for the natural sites (Table 1). All the disturbed sites had significantly greater runoff rates than the natural sites [*Robichaud et al.*, 2010], and the maximum runoff rates were measured in the skid trails. The skid trails also had the greatest sediment flux rates, but the high soil burn severity sites had the greatest runoff velocity [*Robichaud et al.*, 2010]. Three slope classes were used in the experiment, but slope class had no significant effect on

**Table 1.** Site Locations, Historic Annual Rainfall, Dominant Pre-disturbance Vegetation, Duff Thickness, and Soil Texture in the Undisturbed (Natural) Sites for Each Fire Location and the Slope Range, Number of Plots, Mean Runoff Rate, Mean Runoff Velocity, Mean Sediment Flux Rate, Mean Flow Depth, and Mean Flow Width for Each Disturbance Within Each Fire Location[a]

| Location | Latitude and Longitude | Annual Rainfall (mm) | Dominant Over-story Species | Duff (mm) | Soil Texture | Disturbance Class[b] | Slope (%) | Number of Plots | Runoff Rate (L $min^{-1}$) | Runoff Velocity (m $s^{-1}$) | Sediment Flux Rate (kg $s^{-1} \times 10^{-3}$) | Flow Depth (mm) | Flow Width (mm) |
|---|---|---|---|---|---|---|---|---|---|---|---|---|---|
| Tower | 45.00°N 118.75°W | 614[c] | Lodgepole pine (*Pinus contorta*) | 23 | Stony ashy sandy loam | N | 27–79 | 9 | 2.5 | 0.016 | 0.007 | 6.5 | 238 |
| | | | | | | L[d] | 24–52 | 9 | 12 | 0.073 | 0.25 | 6.3 | 282 |
| | | | | | | H[d] | 23–75 | 9 | 20 | 0.29 | 2.7 | 7.2 | 216 |
| | | | | | | S | 24–54 | 6 | 18 | 0.17 | 13 | 13 | 217 |
| North 25 | 47.99°N 120.34°W | 905[c] | Grand fir (*Abies grandis*) | 47 | Gravelly ashy sandy loam | N | 25–66 | 9 | 2.9 | 0.016 | 0.018 | 6.2 | 404 |
| | | | | | | L[d] | 27–64 | 9 | 18 | 0.24 | 1.0 | 7.1 | 233 |
| | | | | | | H[d] | 25–69 | 9 | 21 | 0.33 | 1.1 | 5.7 | 247 |
| | | | | | | S | 18–51 | 6 | 24 | 0.21 | 8.3 | 12 | 109 |

[a] *Robichaud et al.* [2010].
[b] "N" indicates natural, "L" indicates low soil burn severity, "H" indicates high soil burn severity, "S" indicates skid trail.
[c] Period of record was 26 yr for the Tower site and 23 yr for the North 25 site.
[d] The experiments were conducted 10 months after the Tower fire and 2 weeks after the North 25 fire. Differences in runoff rates, runoff velocities, and sediment flux rates were measured between the two low soil burn severity sites but not between the two high soil burn severity sites. The two low soil burn severity disturbances were therefore analyzed as separate disturbance classes while the two high soil burn severity sites were analyzed as the same disturbance class.

runoff rate, runoff velocity, or sediment flux rate [*Robichaud et al.*, 2010]. The data were not separated by slope class in the current analyses. Also, although three different experimental slope lengths (2, 4, and 9 m) were tested at the Tower location, only the 4 m data were used in the current analyses. Because of a decreasing trend in sediment flux rates within many of the inflow rates and disturbance classes, for most of the analyses we used only the later samples and assumed these samples represented the steady state condition [*Robichaud et al.*, 2010]. Significant differences in sediment flux rates were measured between the initial and steady state conditions for nearly all sites (except the Tower low soil burn severity site), indicating the peak rill erosion rates occurred near the onset of runoff.

### 2.4. Calculation of Hydraulic Parameters

[21] The hydraulic shear stress acting on the soil, $\tau_s$, (kg $s^{-2}$ $m^{-1}$) [*Foster et al.*, 1995] was calculated by

$$\tau_s = \gamma R_h \sin\left[\tan^{-1}(S)\right]\frac{f_s}{f_t} \tag{8}$$

where $\gamma$ is the specific weight of water (kg $m^{-2}$ $s^{-2}$), $R_h$ is the hydraulic radius (m), $S$ is the hydraulic gradient, generally assumed to be the slope steepness of the plot (m $m^{-1}$), $f_s$ is the friction due to soil grain and form roughness, and $f_t$ is the Darcy-Weisbach friction factor. The friction due to the soil grain and form roughness can be calculated by

$$f_s = f_t - f_r - f_v \tag{9}$$

where $f_v$ is the friction due to vegetation, assumed zero in our analysis, and $f_r$ is the friction due to residue. The total friction, $f_t$, is

$$f_t = \frac{8gR_hS}{\nu^2} \tag{10}$$

where $g$ is the acceleration due to gravity (m $s^{-2}$) and $\nu$ is the kinematic viscosity ($m^2$ $s^{-1}$). The residue component of friction, $f_r$ can be estimated from

$$f_r = 4.5r_c^{1.55} \tag{11}$$

where $r_c$ is the fraction of the rill covered by residue [*Gilley and Weltz*, 1995]. We assigned a value for the residue cover, $r_c$, for each plot based on the relationship between the amount of total ground cover and duff on the rill surface [*Robichaud*, 2000]. Based on the measured thickness of the duff layer the plots were assigned the following $r_c$ values: 1.0 for all natural plots; 0 for all high soil burn severity and skid trail plots; 0.905 to 1.0 for the Tower low soil burn severity plots; and 0.83 to 1.0 for the North 25 low soil burn severity plots, except for the 3 low slope class plots where the duff thickness was not measured. The 45 L $min^{-1}$ flow rate in one plot at the North 25 low soil burn severity site produced a negative soil shear stress; this value was omitted from further analysis.

[22] The stream power $\Omega$ (kg $s^{-3}$) was

$$\Omega = \gamma R_h V \sin[\tan^{-1}(S)] \tag{12}$$

where $V$ was the measured runoff velocity (m $s^{-1}$). The unit stream power, $\Omega_u$ (m $s^{-1}$), is a function of runoff velocity ($V$) and slope ($S$) and was calculated by the equation

$$\Omega_u = V \sin[\tan^{-1}(S)] \tag{13}$$

[23] The unit length shear force, $\Gamma$ (kg $s^{-2}$), was defined as

$$\Gamma = \gamma A \sin[\tan^{-1}(S)] \tag{14}$$

where $\gamma$ is the specific weight of water (kg m$^{-2}$ s$^{-2}$), $S$ is the rill slope (m m$^{-1}$) and $A$ is the cross-sectional area of the rill (m$^2$) [*Giménez and Govers*, 2002].

[24] From equation (2) the detachment capacity, $D_c$ (kg s$^{-1}$ m$^{-2}$), was defined as the ability of clear flowing water to detach soil particles from the bed and banks of the rill and is calculated by

$$D_c = \frac{-T_c}{wL}\ln\left[1 - \left(\frac{q_s}{wT_c}\right)\left(\frac{D_c^{'}}{D_c^{'} + E}\right)\right] \quad (15)$$

where $L$ is the rill length (m), $w$ is the flow width (m), $T_c$ is the transport capacity of clear flowing water, (kg s$^{-1}$), $q_s$ is the sediment transport rate, (kg s$^{-1}$), $D'_c$ is an iterative solution for the detachment capacity (kg s$^{-1}$ m$^{-2}$), and $E$ is the sediment added from inter-rill flow into the rill (kg s$^{-1}$ m$^{-2}$) [*Elliot et al.*, 1989]. In the current experiment we assumed the inter-rill addition to the rill flow and the resultant inter-rill sediment supply were zero, simplifying equation (15) to

$$D_c = -\frac{T_c}{wL}\ln\left(1 - \frac{q_s}{wT_c}\right) \quad (16)$$

[25] The transport capacity, $T_c$ (kg s$^{-1}$), was calculated using a derivation from Yalin's bed load transport theory [*Yalin*, 1963] as modified for the WEPP model [*Foster and Meyer*, 1972]

$$T_c = wB\tau_s^{1.5} \quad (17)$$

where $w$ was the flow width (m) and $B$ was the transport coefficient (s$^2$ m$^{0.5}$ kg$^{-0.5}$). *Elliot et al.* [1989] present estimates for values of $B$ for 36 agricultural soils; the range of calculated $B$ values was 0.077 to 0.11 s$^2$ m$^{0.5}$ kg$^{-0.5}$. The soil in the *Elliot et al.* [1989] data set that was most comparable to the soils at the Tower and North 25 locations had a $B$ value of 0.098 s$^2$ m$^{0.5}$ kg$^{-0.5}$ (Whitney soil series), so we used this value in our computations. Selecting the extreme values from the WEPP data set [*Elliot et al.*, 1989] would yield transport capacities that were 21% lower or 12% greater than the calculated values, respectively, as the relation between $B$ and the transport capacity is linear. We found that the calculated $K_r$ values were not sensitive to changes in $B$ within this range in this study.

[26] For the data set presented in part 1 of this study [*Robichaud et al.*, 2010], the stream power rill erosion model (equation (5)) also can be simplified. Assuming the flow is constant, the first term on the left side of the equation is the change in sediment flux with distance, or the sediment detachment per unit length, $D_L$ (kg s$^{-1}$m$^{-1}$). The volumetric flow rate, $Q$, was constant for a given rill and inflow condition, so $dQ/dx$ was zero. There was no observed deposition in the steep rill plots, so $H$ was zero and the term [$(1 - H)\ W_b + W_s$] became the flow width $w$. Furthermore, with the assumption of no inter-rill erosion, the final inter-rill term also was zero. To estimate the fraction of excess stream power available for detachment and transport, $F$, *Hairsine and Rose* [1992b] used data from the transport limited condition of a simulated rainfall experiment. The experiment in part 1 of this study [*Robichaud et al.*, 2010] did not include rainfall, so it was not possible to estimate $F$ by this method. Rather, we combined $F$ with $J$ for a forest soil erodibility term for the stream power model, $K_\Omega$

$$K_\Omega = \frac{F}{J} \quad (18)$$

[27] Finally, all of the plots had the same length (4 m), so we calculated the rill erodibility values using the sediment flux rate, $q_s$

$$q_s = K_\Omega(\Omega - \Omega_0) \quad (19)$$

where $K_\Omega$ took the units s$^2$. To directly compare unit stream power, the unit length shear force, and shear stress erodibility values, we substituted each of these hydraulic parameters for the stream power in equation (19) to also calculate rill erodibility values based on unit stream power, $K_{\Omega u}$ (kg m$^{-1}$), unit length shear force, $K_\Gamma$ (s), and shear stress, $K_\tau$ (s m). Two of the rill erodibility parameters ($K_\Omega$ and $K_\Gamma$) were divided by the rill length (4 m) to compare them to other published values.

[28] The sediment flux rate, $q_s$, (kg s$^{-1}$) was divided by the transport capacity, $T_c$ (kg s$^{-1}$), and this value was termed the transport ratio and used to compare the sediment flux rate directly to the transport capacity. The transport ratios were calculated for each inflow rate and disturbance. We assumed a water temperature of 20°C to determine specific weight, $\gamma$, and kinematic viscosity, $\nu$.

[29] Runoff and sediment flux rates were measured for each plot, inflow rate, and sample. For each plot and inflow rate, the runoff velocity, flow width, and flow depth were measured and the hydraulic radius, soil shear stress, stream power, unit stream power, unit length shear force, transport capacity, detachment capacity, and transport ratio were calculated.

### 2.5. Statistical Analyses

[30] The SAS statistical software was used for all statistical analyses [*SAS Institute*, 2008]. Differences in the four hydraulic parameters (soil shear stress, $\tau_s$, stream power, $\Omega$, unit stream power, $\Omega_u$, and unit length shear force, $\Gamma$) among the disturbance classes were tested using a generalized linear mixed model with each of these hydraulic variables as the dependent variable, disturbance type as the independent class variable, and plot replicate and fire location as a random variable [*Littel et al.*, 2006]. Each dependent variable was modeled with the lognormal distribution. The differences among the disturbance levels for all mixed-effects models were tested using least squares means with a Tukey-Kramer adjustment [*Ott*, 1993].

[31] We used simple linear regression to determine which of the four hydraulic parameters (soil shear stress, $\tau_s$, stream power, $\Omega$, unit stream power, $\Omega_u$, and unit length shear force, $\Gamma$) best predicted the sediment flux rate, $q_s$, and sediment detachment capacity, $D_c$. All the variables in this analysis were log-transformed to improve the normality of the modeled residual errors [*Helsel and Hirsh*, 2002]. A small value was added to the sediment flux ($5 \times 10^{-9}$ kg s$^{-1}$) and unit stream power (0.001 m s$^{-1}$) so that zero-value data, resulting from the no runoff condition, could be log-transformed.

**Table 2.** Mean Steady State Soil Shear Stress, Stream Power, Unit Stream Power, Unit Length Shear Force, Number of Rills, Hydraulic Radius, Sediment Flux Rate, and Detachment Capacity for Each Location and Disturbance Class[a]

| Disturbance Class | $n$ | $\tau_s = \gamma R_h \sin[\tan^{-1}(S)]_{f_i}^{f_t}$ (kg s$^{-2}$ m$^{-1}$) | $\Omega = \gamma R_h V \sin[\tan^{-1}(S)]$ (kg s$^{-3}$) | $\Omega_u = V \sin[\tan^{-1}(S)]$ (m s$^{-1}$) | $\Gamma = \gamma A \sin[\tan^{-1}(S)]$ (kg s$^{-2}$) | Number of Rills | $R_h$ (m × 10$^{-3}$) | $q_s$ (kg s$^{-1}$ × 10$^{-3}$) | $D_c$ (kg s$^{-1}$ m$^{-2}$ × 10$^{-3}$) |
|---|---|---|---|---|---|---|---|---|---|
| Natural | 12 | 17 A | 1.1 B | 0.006 C | 5.2 A | 1.7 | 5.8 | 0.013 D | 0.025 A |
| Low soil burn severity (Tower) | 20 | 20 A | 2.7 B | 0.027 B, C | 8.4 A | 1.3 | 6.2 | 0.21 C | 0.29 B |
| Low soil burn severity (North 25) | 26 | 22 A | 5.4 A | 0.088 A | 5.9 A | 2.5 | 6.0 | 1.0 A, B | 1.0 A, B |
| High soil burn severity | 89 | 23 A | 7.0 A | 0.12 A | 5.7 A | 2.6 | 5.6 | 1.9 A, B | 3.2 A, B |
| Skid trails | 57 | 31 A | 6.3 A | 0.062 A, B | 6.1 A | 1.7 | 9.2 | 11 A | 29 B |
| | | | | *Coefficient of Determination $R^2$* | | | | | |
| Log ($q_s$) | 195 | 0.18 | 0.41 | 0.25 | 0.006 | | | | |
| Log ($D_c$) | 194 | 0.20 | 0.38 | 0.22 | 0.007 | | | | |

[a]Here $\tau_s$, mean steady state soil shear stress (equation (8)); $\Omega$, stream power (equation (12)); $\Omega_u$, unit stream power (equation (13)); $\Gamma$, unit length shear force (equation (14)); $R_h$, hydraulic radius; $q_s$, sediment flux rate; and $D_c$, detachment capacity (equation (16)). Letters A, B, or C indicate significantly different means within that column ($\alpha = 0.05$). The hydraulic radius is the mean value for all identified rills at each inflow rate, plot, and site. The $R^2$ values between the log-transformed soil shear stress, $\tau_s$, stream power, $\Omega$, unit stream power, $\Omega_u$, and unit length shear force, $\Gamma$, and log-transformed sediment flux rate, $q_s$, and log-transformed detachment capacity, $D_c$, are shown at the bottom.

[32] A simple linear regression between the sediment detachment capacity ($D_c$) and soil shear stress, $\tau_s$, was used to calculate the rill erodibility, $K_r$, and critical shear stress, $\tau_c$, for the shear stress model (equation (2)). The regression took the form

$$y = \beta_0 + \beta_1 x \tag{20}$$

where the slope ($\beta_1$) of the regression line was the rill erodibility parameter, $K_r$, and the x-intercept ($-\beta_0/\beta_1$) was the critical soil shear stress, $\tau_c$ [*Alberts et al.*, 1995; *Knapen et al.*, 2007]. A similar regression was conducted between the sediment flux rate, $q_s$, and the four hydraulic parameters to calculate their respective rill erodibility coefficients. Confidence intervals for the shear stress model's erodibility, $K_r$, and critical shear stress, $\tau_c$, were calculated using standard methods for linear regression and a regression calibration procedure, respectively [*Ott*, 1993]. The significance level ($\alpha$) was 0.05 for each statistical test or calculation.

## 3. Results

[33] Unlike the significant differences in runoff rates, runoff velocities, and sediment flux rates measured among the disturbance classes in part 1 of this study (Table 1), there was no difference in soil shear stress, $\tau_s$, or unit length shear force, $\Gamma$, among the disturbance classes (Table 2). There were some differences in stream power, $\Omega$, among disturbances; notably the natural sites had less stream power (1.1 kg s$^{-3}$) than all of the disturbed sites (5.4 to 7.0 kg s$^{-3}$) except for the Tower low soil burn severity site (2.7 kg s$^{-3}$). The unit stream power, $\Omega_u$, followed a similar pattern as the stream power, except that the difference between the Tower low soil burn severity site (0.027 m s$^{-1}$) and the skid trail site (0.062 m s$^{-1}$) was not significant (Table 2). There was no difference in stream power or unit stream power among the high soil burn severity, skid trail, or the North 25 low soil burn severity sites (Table 2). The stream power best predicted the log-transformed sediment flux rate and soil detachment capacity, with $R^2$ values of 0.41 and 0.38, respectively (Table 2).

[34] The calculated transport capacity ranged from 2.0 to 3.1 kg s$^{-1}$ among the disturbance classes (Table 3) which indicates all the disturbance classes had sufficient energy to transport the eroded sediment. For each disturbance class, the mean sediment flux rate was much less than the mean transport capacity, resulting in a maximum transport ratio of 0.5% (Table 3). The sediment transport in each disturbance class was clearly source limited. The soil resisted additional particle detachment even though there was ample energy in the runoff to transport additional sediment. Also, although the sediment transport capacity dropped when the inflow rate was reduced to 14 L min$^{-1}$ (Figure 1), so did the sediment flux rates, resulting in a maximum transport ratio of only 0.14% in the skid trail plots at the 14 L min$^{-1}$ inflow rate. In this flow regime, net sediment deposition would still be minimal, and the factor limiting sediment flux rate would be the sediment detachment.

[35] The detachment capacity versus shear stress rill erodibility, $K_r$, values varied over four orders of magnitude among the five disturbance classes (Figure 2). The natural sites had the smallest erodibility values (1.5 × 10$^{-6}$ s m$^{-1}$), and the erodibility values increased with increasing disturbance. The erodibility values in the low soil burn severity sites were negative, and as these results were not physically realistic, this may have been a result of the relatively narrow range of soil shear stress values applied (Figure 2). The value for the high soil burn severity sites was 2.0 × 10$^{-4}$ s m$^{-1}$ and the erodibility in the skid trail sites was 1.7 × 10$^{-3}$ s m$^{-1}$. The critical shear stress, $\tau_c$, was only calculable for the high soil

**Table 3.** Mean Transport Capacity, $T_c$, and Transport Ratio, $q_s/T_c$, for Each Location and Disturbance Class[a]

| Disturbance Class | $n$ | $T_c$ (kg s$^{-1}$) | $q_s/T_c$ (%) |
|---|---|---|---|
| Natural | 12 | 2.0 | 0.002 |
| Low soil burn severity (Tower) | 20 | 2.6 | 0.031 |
| Low soil burn severity (North 25) | 26 | 2.7 | 0.059 |
| High soil burn severity | 89 | 2.5 | 0.11 |
| Skid trails | 52 | 3.1 | 0.53 |

[a]For $T_c$, see equation (17).

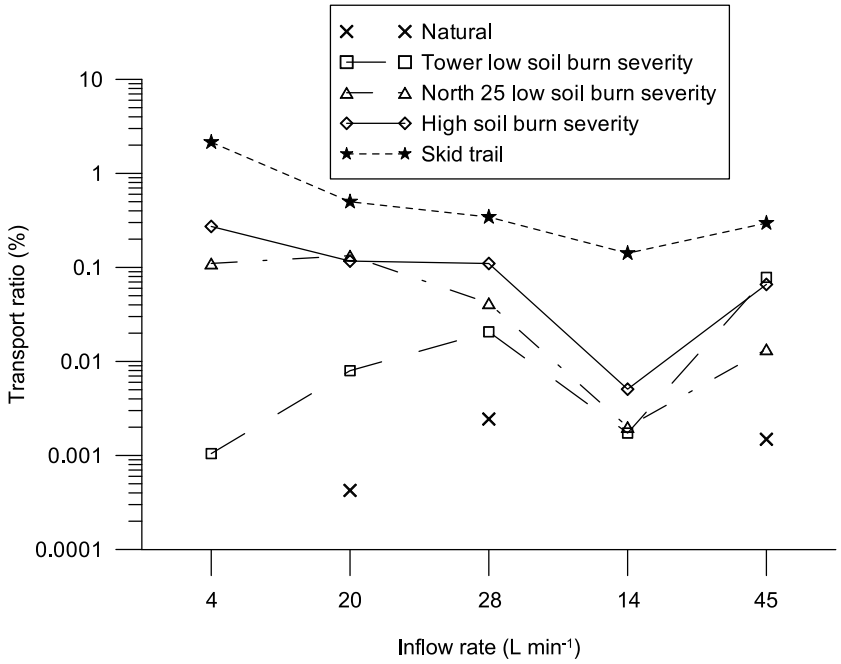


**Figure 1.** Transport ratio versus inflow rate for the five disturbance classes.

burn severity and the skid trail sites, and neither of these two values (6.3 and 15 kg $s^{-2}$ $m^{-1}$, respectively) was significantly different from zero (Figure 2). For the 3 disturbance classes where the $K_r$ was positive, the $K_r$ values calculated from the initial samples were slightly higher than the values calculated for the assumed steady state condition (Figure 2).

[36] When the data were combined across the disturbance classes, the soil shear stress, $\tau_s$, was the best predictor of the sediment flux rate, and this regression produced an $R^2$ value of 0.42 (Table 4). When individual disturbance classes were considered, the results were less conclusive, as the sediment flux rates in the lesser disturbed classes were better predicted with the stream power, $\Omega$, or unit stream power, $\Omega_u$, and the more disturbed classes were better predicted with the soil shear stress (Table 4). The best predictor of sediment flux rates in the natural sites was unit stream power (an $R^2$ of 0.66) (Table 4). The best predictor in the low soil burn severity sites was the stream power (an $R^2$ of 0.64 for Tower and an $R^2$ of 0.10 for North 25) (Table 4). The unit length shear force, $\Gamma$, produced significant coefficients only for the data combined across disturbances and for the skid trail sites (Table 4), and all of the other hydraulic parameters produced better $R^2$ values for this disturbance class than the unit length shear force.

[37] The metal tracks of the skidder left depressions of 8–12 cm in depth, which had greater compaction than the adjacent areas. These depressions effected an inferred change in the surface roughness caused by the small steps and pools in the flow path. The change to the flow path in the skid track also resulted in nick points and flow that was both deeper and sometimes narrower than was measured in the high soil burn severity sites (Table 1).

[38] The data presented in Tables 2 and 4 may seem contradictory, with Table 2 indicating that the stream power was a better predictor of sediment flux and Table 4 indicating the shear stress was a better predictor of sediment flux. Upon closer inspection of the methods, however, all the data in Table 2 were log-transformed and the data in Table 4 were not transformed. We believe the analysis leading to Table 2 is more statistically correct, as all the data display some non-uniformity of variance before the log-transformations; so the findings presented in Table 2 are the preferred method for making final assessments of predictability. Table 4 presents the linear relationships that have been applied in previous models, and so can be used to compare the current data to previous studies. As the data in Table 4 were not normally distributed, however, the assumptions for regression are not completely met and at the least, the statistical power has been reduced.

## 4. Discussion

### 4.1. Transport or Detachment Limited Flow Regimes

[39] As indicated in Table 3, all sediment flux rates were much lower than the calculated transport capacities, indicating the erosion rates were not limited by the transport capacity but by the detachment capacity of the flowing water. The large calculated transport capacities suggest the sediment load could be increased by orders of magnitude without resulting in net deposition. In a natural runoff event, additional sediment would be supplied by inter-rill erosion, but even with the added sediment supply, these systems may not achieve the transport capacity without some change in location (e.g., at the toe of a hillslope or in a small depression where the slope decreases), flow geometry (e.g., if the rill split into multiple flow paths), or sediment source.

[40] The decoupling of inter-rill erosion and rill erosion in this experiment allowed us to calculate the rill erosion parameters, but this led to some limits on the interpretation of the results. According to the *Foster and Meyer* [1972]

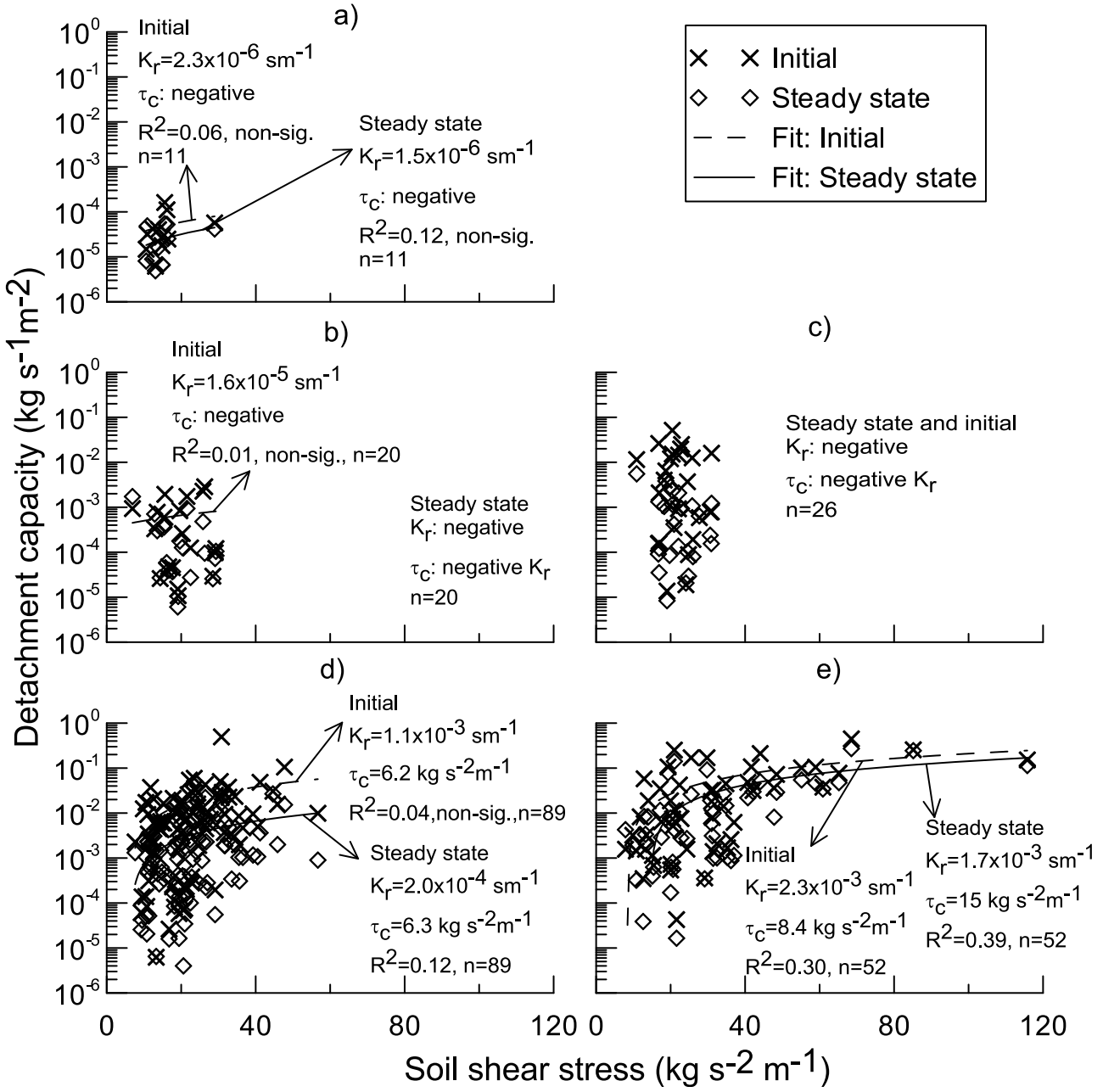


**Figure 2.** Detachment capacity versus soil shear stress for the five disturbance classes: (a) natural, (b) Tower low soil burn severity, (c) North 25 low soil burn severity, (d) high soil burn severity, and (e) skid trails. All plots share the common legend in a) ("x" represents initial condition, diamond represents steady state condition). The log scale is used for presentation only; all regressions were conducted on non-transformed data and were of the form in equation (20). Rill erodibility, $K_r$ ($\beta_1$ in equation (20)), and critical shear stress, $\tau_c$ ($-\beta_0/\beta_1$ in equation (20)), are shown where they had positive sign.

**Table 4.** Sediment Flux Rill Erodibility Coefficients, $K$, for the Four Hydraulic Models and Five Disturbance Classes[a]

| Disturbance Class | $K_\tau$ Soil Shear Stress (s m) | $K_\Omega$ Stream Power ($s^2$) | $K_{\Omega u}$ Unit Stream Power (kg $m^{-1}$) | $K_\Gamma$ Unit Length Shear Force (s) |
|---|---|---|---|---|
| Natural | negative | $4.0 \times 10^{-6}$ (0.02) | **$1.6 \times 10^{-3}$ (0.66)** | $6.3 \times 10^{-7}$ (0.01) |
| Low soil burn severity (Tower) | negative | **$3.2 \times 10^{-4}$ (0.64)** | **$1.5 \times 10^{-2}$ (0.55)** | $7.3 \times 10^{-5}$ (0.18) |
| Low soil burn severity (North 25) | negative | **$1.7 \times 10^{-4}$ (0.10)** | $7.1 \times 10^{-3}$ (0.03) | negative |
| High soil burn severity | **$1.1 \times 10^{-4}$ (0.16)** | **$2.1 \times 10^{-4}$ (0.11)** | **$9.9 \times 10^{-3}$ (0.04)** | $6.3 \times 10^{-6}$ (0.0001) |
| Skid trails | **$6.5 \times 10^{-4}$ (0.58)** | **$2.3 \times 10^{-3}$ (0.46)** | **0.27 (0.25)** | **$1.6 \times 10^{-3}$ (0.24)** |
| All classes | **$5.2 \times 10^{-4}$ (0.42)** | **$8.9 \times 10^{-4}$ (0.15)** | $1.2 \times 10^{-2}$ (0.01) | **$5.2 \times 10^{-4}$ (0.06)** |

[a]The dependent variable was sediment flux rate, $q_s$ (kg $s^{-1}$) (equation (19)). Coefficients were calculated using the assumed steady state condition. $R^2$ values are shown in parentheses; bold indicates the coefficient was significantly different than 0 at $\alpha = 0.05$.

model, the clean water supply may have produced more erosion in the rills than would naturally occur since there was no entrained sediment to reduce the detachment capacity of the flowing water (equation (15)), or would have resulted in less deposition according to the *Hairsine and Rose* [1992b] model. Considering the relatively low transport ratios (Table 3), there was ample energy to transport additional sediment and so the difference in scouring capacity between our clean water supply and typical sediment-carrying runoff may be minimal. Still, the artificially high erosive condition may have produced the greatest rill erosion rates [*Foster*, 1982].

### 4.2. Detachment Capacity and Transport Capacity

[41] The ability to transport additional sediment is important in natural settings where rain splash and inter-rill erosion occur and runoff is sediment laden before it converges into rill flow. In this case, especially on lower slopes such as near the valleys or toes of the slopes, net deposition would occur if the transport capacity rates were exceeded. The calculated detachment capacities ($2.5 \times 10^{-5}$ to 0.029 kg $s^{-1}$ $m^{-2}$) (Table 2) were less and the transport capacities (2–3.1 kg $s^{-1}$) (Table 3) were greater than values reported for agricultural soils. For example, the mean detachment capacity in the rainfall simulation study on the Whitney loam, a soil with similar texture and mineralogy to the soils in this study, was 0.052 kg $s^{-1}$ $m^{-2}$ and the transport capacity averaged 0.18 kg $s^{-1}$ from 6 plots with 7 percent slopes (calculated from *Elliot et al.* [1989]). These large differences in detachment capacity and transport capacity in forest soils compared to agriculture soils suggest that care must be taken before applying erosion models developed for agricultural soils to steep forested hillslopes. These results suggest that both the *Foster and Meyer* [1972] model, where detachment is limited by sediment in transport, and the *Hairsine and Rose* [1992a, 1992b] model, where sufficient sediment is entrained to result in significant deposition processes occurring within eroding rills, may not apply to steep forested slopes. This observation supports the assumption that the value for the fraction of the rill bottom, $H$, that is covered with deposited sediment in the *Hairsine and Rose* [1992a, 1992b] model (equation (5)) is likely near zero for all of the conditions presented in this paper. It also means that the observed unit area erosion rate, $D_r$, would lead to similar erodibility values as the detachment capacity, $D_c$, which assumes sediment detachment may be limited by sediment in transport. An inspection of equation (3) shows that as the ratio of sediment in transport to transport capacity approaches zero, the ratio of detachment rate to detachment capacity approaches 1. The *Giménez and Govers* [2002] model (equation (7)) assumes that sediment in transport does not affect detachment except at very high sediment transport rates, and so the relatively low amounts of sediment in transport in this study should have no impact on the performance of their model.

### 4.3. Rill Roughness and Velocity

[42] The increased roughness in the skid trails was a result of the changes in the soil surface caused by the metal cleats on the tracks of the skidder. We measured the greatest values of depth, hydraulic radius, and shear stress, in the skid trails as compared to the other disturbance classes (Tables 1 and 2). Another effect was that the depressions slowed the runoff, resulting in a lower velocity and therefore smaller stream power and unit stream power values in the skid trails as compared to the high soil burn severity sites, the only other disturbance with no vegetation or duff. The rill erodibility values were all highest for the skid trails as compared to the other disturbance classes (Table 4). The skid trails had the best $R^2$ of all the disturbance classes for the shear stress rill erodibility (Figure 2) and produced some of the highest $R^2$ values between the individual hydraulic parameters, especially shear stress, and the sediment flux rates (Table 4).

[43] The rill roughness in these undisturbed forest sites were much higher than in most agricultural studies where primary and secondary tillage generally are carried out before the experiment [*Elliot et al.*, 1989; *Laflen et al.*, 1991; *Hairsine and Rose*, 1992a, 1992b]. This increase in roughness would likely decrease the amount of shear stress available to detach sediment in the shear stress model (equation (8)) and the fraction of energy available to detach and transport sediment (($F$) in equation (5)).

### 4.4. Erodibility Estimates

[44] With a more disparate selection of forest soils our experiments may have produced a wider range of $K_r$ values in the natural sites. The $K_r$ values we calculated for the natural sites were 3 to 4 orders of magnitude smaller than the values calculated to parameterize the WEPP model for agricultural conditions, which ranged from 0.0012 to 0.045 s $m^{-1}$ [*Elliot et al.*, 1989]. The low values in the natural sites were not unexpected, as the forest soils in the current study were previously undisturbed and the soils used to parameterize the WEPP model for agriculture all had been recently plowed.

[45] The maximum calculated $K_r$ was 0.0017 s $m^{-1}$ in the skid trail sites, which was an order of magnitude smaller than the $K_r$ value for the Whitney agricultural soil (0.023 s $m^{-1}$) [*Elliot et al.*, 1989] and was near the median $K_r$ (0.004 s $m^{-1}$) for the agricultural field data compiled by *Knapen et al.* [2007]. The calculated $K_r$ values for the skid trails also fell within the range of $K_r$ values calculated for a range of flow depths over forest roads (0.00049 to 0.0076 s $m^{-1}$) [*Foltz et al.*, 2008]. For the stream power model, our maximum $K_\Omega$ per unit length was $5.8 \times 10^{-4}$ $s^2$ $m^{-1}$ (skid trails), compared to 0.004 to 0.008 $s^2$ $m^{-1}$ for the three agricultural soils modeled by *Hairsine and Rose* [1992b] and 0.002 to 0.049 $s^2$ $m^{-1}$ for the nine agricultural soils reported by *Elliot and Laflen* [1993]. Similarly, our maximum $K_\Gamma$ per unit length was greatest for the skid trails and this value was 0.0004 s $m^{-1}$, compared to the values 0.017 and 0.018 s $m^{-1}$ for silt loam and loamy sand, respectively, reported by *Giménez and Govers* [2002].

[46] The disturbance of the forest soil as a result of the metal-tracked skidder was therefore sufficient to increase the erodibility of these soils to a degree consistent with that of a recently tilled agricultural field, or a low-use native surface road, and an order of magnitude greater than the calculated erodibility values in the fire-disturbed sites. Current forest best management practices (BMPs) are well justified that require forest managers to incorporate mitigation treatments, such as installing water bars or mulch on

skid trails, or developing timber management plans that minimize the number of skid trails, thereby reducing the effects of this disturbance.

[47] The low and high soil burn severity sites had $K_r$ values that were one to two orders of magnitude greater than the natural sites. Our calculated $K_r$ values for the low and high soil burn severity sites were at least an order of magnitude smaller than an average $K_r$ value reported for burned range land [*Moffet et al.*, 2007]; however, the $K_r$ values for the two natural sites also were one or two orders of magnitude smaller than the value $K_r$ reported for unburned range land in an Agricultural Research Service range land erodibility study [*Laflen et al.*, 1991] and in the *Moffet et al.* [2007] study. It has been well documented that erosion rates from burned forests are generally much greater than the rates from adjacent undisturbed areas, and often the increases are one to two (or more) orders of magnitude [e.g., *Benavides-Solorio and MacDonald*, 2001; *Sheridan et al.*, 2007]. Our measured rill erodibility values help explain the previously reported orders of magnitude increases in sediment yields from burned areas.

[48] We calculated large differences in $K_r$ between the natural sites and the disturbed sites (Figure 2), as well as large differences in $K_r$ among the types of disturbance. This suggests that the disturbance has more impact on $K_r$ than subtle differences in soil type. In a study comparing inter-rill erodibility parameters in disturbed forests, *Robichaud* [1996] found similar order of magnitude increases in the inter-rill erodibility between the natural and burned or skid trail plots. Therefore future erosion modeling efforts for forest disturbances should focus less on the precision of the estimate of erodibility for the undisturbed areas and more on attaining a reliable order of magnitude estimate of erodibility in the disturbed areas.

[49] The critical shear stress, $\tau_c$, values were positive only for the two most disturbed of the five disturbance classes, and these two values were not significantly different from zero (Figure 2). This implies that erosion in forests may commence immediately upon application of a small erosive force and that in steep forest environments the critical shear stress dependent detachment capacity concept may not adequately describe the transport mechanism; however, considering the relatively low number of replicates in this study and the resultant high variability in shear stress and detachment capacity data, this was not conclusive.

### 4.5. Transient Nature of Rill Erosion

[50] The larger $K_r$ values for the initial samples as compared to the steady state values suggest that the rill erodibility parameter should not be held constant for the duration of a given flow event. Although we cannot define the shape of the rill erodibility as a function of time (or amount of antecedent flow or erosion) with the current data set, it clearly would decrease over a short period of time within a fixed flow rate, and the response curve likely would be similar to that proposed by *Moffet et al.* [2007] or *Foltz et al.* [2008].

[51] One explanation for the changes in $K_r$ over time is that the erodibility changes in response to changes in the available sediment. This explanation is similar to some of the theory behind the *Hairsine and Rose* [1992b] model, except in that model the erodibility changes as the bed of the rill changes from cohesive soils to non-cohesive sediments. Our results suggest a similar modeling approach may be warranted, but with a model that changes the erodibility of the bed from one of lower cohesion to one of higher cohesion as a function of prior sediment detachment. With more available sediment, for example at the beginning of a runoff event or in a highly disturbed site, the $K_r$ values would be high. As easily eroded soil is removed, more erosion-resistant (larger or more embedded) soil particles are exposed, and therefore the $K_r$ decreases. The general shape of the $K_r$ response curve throughout a runoff event could therefore be modeled based on the disturbance type. The changes in $K_r$ may not be apparent in areas with a much larger supply of mobile sediment, such as recently tilled agricultural fields, in mine tailings piles, in active construction sites, or in our case, in recently created skid trails. For example, an early analysis of the *Elliot et al.* [1989] agricultural data set did not show any general trend in reduced erosion associated with flow rates later in the experiment. They did, however, reach the layer compacted by the plow in one plot and there the erosion rapidly decreased. This higher flow rate was not used in further analysis (the Woodward soil in the work by *Elliot et al.* [1989]).

### 4.6. Comparison of Rill Erosion Models

[52] In calculating the WEPP erodibility parameter, the rill erodibility, $K_r$, values varied by orders of magnitude among the disturbance classes, but the soil shear stress, $\tau_s$, remained relatively constant. This suggests that a different hydraulic parameter may be a better predictor of sediment production. Our analysis of the four hydraulic parameters indicated that the stream power was the best overall predictor of sediment flux rate and sediment detachment capacity (Table 2). In three agricultural studies, other parameters besides the shear stress were better predictors of the observed erosion: *Elliot and Laflen* [1993] also found that the stream power model was better than shear stress; *McIsaac et al.* [1992] preferred unit stream power; and *Giménez and Govers* [2002] determined that the unit length shear force model was the best fit.

[53] In comparing the linear relations in Table 4 it appears that the models were not consistently robust under the lower erodibility and source-limited conditions on our steep forest plots. The shear stress model was the best linear fit to the combined data and had the highest $R^2$ value for the skid trail sites, but did not produce positive slopes for the natural or low soil burn severity sites. The stream power and unit stream power models produced positive slopes for all regressions, but the $R^2$ varied considerably for the different disturbance classes. The unit length shear force produced a negative slope for the North 25 low soil burn severity class, and all of its $R^2$ values were below 0.25. As a whole, the models worked the best when the erosion rates were very low and the runoff velocity was the dominant factor (natural and Tower low soil burn severity sites), or very high when the flow depth was the dominant factor (skid trails). None of the models explained much of the variability in sediment flux rates for the North 25 low soil burn severity site or the high soil burn severity sites—the disturbance classes with sediment flux rates in the middle of the measured range (Table 2).

[54] The unit length shear force model produced the lowest $R^2$ values (Table 4). This may be because the unit length shear force depends on an estimate of the rill cross-sectional area and we assumed a rectangular cross section. The shapes of the rills likely varied considerably among and within the plots as the concentrated flow dispersed and re-concentrated as it meandered down the hill. Characterization of the shape of the rill or more careful site selection where flow dispersion would be less likely would have resulted in more accurate assessments of rill area and hydraulic radius, and it is possible the three models that depend on the rill geometry (soil shear stress, stream power, and unit length shear force) would have performed better.

[55] Our study is not the only data set with dynamic rill erodibility properties, and there is a need for advanced rill erosion studies to focus on dynamic erosion processes common on soils with changing roughness [*Elliot et al.*, 1989], limited sediment [*Foltz et al.*, 2008], or changing rill shapes (this study).

## 5. Conclusions

[56] Concentrated flow in rills is one of the transport paths for eroded soil to reach the larger stream network. Erosion also occurs within the rills and in this two-part study we quantified the rill erosion rates, identified some of the processes controlling the erosion, and related the measured erosion rates and hydraulic conditions to modeling parameters used in four rill erosion models. The data indicated that the simulated runoff on steep natural and disturbed (10-month old low soil burn severity, 2-week old low soil burn severity, high soil burn severity, and logging skid trails) forested hillslopes had very high sediment transport capacities and therefore was detachment limited. The calculated rill erodibility parameters increased by orders of magnitude with increasing disturbance, depending on the controlling hydraulic variable used (soil shear stress, $\tau_s$, stream power, $\Omega$, unit stream power, $\Omega_u$, or unit length shear force, $\Gamma$). For the detachment capacity versus soil shear stress, the erodibility parameter, $K_r$, ranged from $1.5 \times 10^{-6}$ s m$^{-1}$ in the natural plots to $2.0 \times 10^{-4}$ s m$^{-1}$ in the high soil burn severity plots, to $1.7 \times 10^{-3}$ s m$^{-1}$ in the logging skid trail plots. While the log-transformed stream power was the best of the four hydraulic parameters (soil shear stress, $\tau_s$, stream power, $\Omega$, unit stream power, $\Omega_u$, and unit length shear force, $\Gamma$) at predicting the log-transformed sediment flux rates ($R^2 = 0.41$), no single hydraulic parameter consistently predicted the sediment flux across the five disturbance classes. The unit length shear force model did not perform as well as the shear stress, stream power, or unit stream power models in the current study.

[57] In the three disturbance classes where comparisons could be made (natural, high soil burn severity, and skid trails), the $K_r$ decreased from the initial condition to the steady state condition within a given inflow rate. These results indicate that the rill erodibility values for modeling erosion in disturbed forests should not be held constant for a given runoff event.

[58] Our calculated rill erodibility values help explain the previously reported orders of magnitude increases in erosion in burned areas as compared to natural areas. The results of this study suggest that further research in dynamic rill erosion are warranted to better understand and model how changing sediment availability, changing channel shapes, and changing channel roughness affect rill erosion processes.

## Notation

$G$ sediment load per unit width, kg s$^{-1}$ m$^{-1}$.
$D_r$ rill erosion rate, kg s$^{-1}$ m$^{-2}$.
$D_i$ inter-rill erosion rate, kg s$^{-1}$ m$^{-2}$.
$D_c$ detachment capacity for rills, kg s$^{-1}$ m$^{-2}$.
$T_c$ transport capacity, kg s$^{-1}$.
$w$ flow width, m.
$L$ rill length, m.
$q_s$ sediment flux rate, kg s$^{-1}$.
$\tau_s$ soil shear stress, kg s$^{-2}$ m$^{-1}$.
$\gamma$ specific weight of water, kg m$^{-2}$ s$^{-2}$.
$g$ acceleration due to gravity, 9.81 m s$^{-2}$.
$R_h$ hydraulic radius, m.
$d$ flow depth, m.
$S$ rill slope, m m$^{-1}$.
$f_s$ friction due to soil grain and form roughness, no units.
$f_t$ Darcy-Weisbach friction factor, no units.
$f_r$ friction due to residue, no units.
$f_v$ friction due to vegetation, no units.
$\nu$ kinematic viscosity of water at 20°C, $1.004 \times 10^{-6}$ m$^2$ s$^{-1}$.
$r_c$ fraction of rill covered by residue material, no units.
$K_r$ rill erodibility, s m$^{-1}$.
$\tau_c$ critical shear stress, kg s$^{-2}$ m$^{-1}$.
$Q$ volumetric flow rate, m$^3$ s$^{-1}$.
$c_i$ sediment concentration of particle size class $i$, kg m$^{-3}$.
$H$ fraction of the rill wetted perimeter base covered by deposited sediment, m m$^{-1}$.
$W_b$ width of the base of a trapezoidal rill, m.
$W_s$ horizontal width of the sides of a trapezoidal rill, m.
$\Omega$ stream power, kg s$^{-3}$.
$V$ runoff velocity, m s$^{-1}$.
$\Omega_0$ (critical) stream power below which no entrainment occurs, kg s$^{-3}$.
$F$ fraction of stream power used in entraining or re-entraining sediment in class size $i$.
$I$ number of settling velocity classes.
$J$ specific energy of entrainment, m$^2$ s$^{-2}$.
$q_{syi}$ inter-rill contribution of sediment to the rill, kg s$^{-1}$ m$^{-1}$.
$K_{\Omega u}$ unit stream power rill erodibility, kg m$^{-1}$.
$\Omega_u$ unit stream power, m s$^{-1}$.
$\Omega_{u0}$ (critical) unit stream power below which no erosion occurs, m s$^{-1}$.
$D_L$ sediment flux per unit length of rill, kg s$^{-1}$ m$^{-1}$.
$\Gamma$ unit length shear force, kg s$^{-2}$.
$A$ cross-sectional area of the rill, m$^2$.
$K_\Omega$ stream power rill erodibility for sediment flux, s$^2$.
$K_\Gamma$ unit length shear force erodibility for sediment flux, s.
$K_\tau$ shear stress rill erodibility for sediment flux, s m.

[59] **Acknowledgments.** Funding for this project was provided by the U.S. Department of Agriculture, Forest Service, Rocky Mountain Research Station. Bob Brown, Chi-hua Huang, Mark Nearing, Richard Wood-Smith, Craig Busskohl, the editor and assistant editor, and three anonymous reviewers provided insightful advice, discussion, or comments.

## References

Alberts, E. E., M. A. Nearing, M. A. Weltz, L. M. Risse, F. B. Pierson, X. C. Zhang, J. M. Laflen, and J. R. Simanton (1995), Soil component,

USDA-Water Erosion Prediction Project: Hillslope profile and watershed model documentation, *Rep. 10*, chap. 7, pp. 7.1–7.47, Natl. Soil Erosion Res. Lab., West Lafayette, Indiana.

Benavides-Solorio, J., and L. H. MacDonald (2001), Post-fire runoff and erosion from simulated rainfall on small plots, Colorado Front Range, *Hydrol. Processes*, *15*, 2931–2952, doi:10.1002/hyp.383.

Bryan, R. (2000), Soil erodibility and processes of water erosion on hillslope, *Geomorphology*, *32*, 385–415, doi:10.1016/S0169-555X(99)00105-1.

Burroughs, E. R., Jr., C. H. Luce, and F. Phillips (1992), Estimating interrill erodibility of forest soils, *Trans. ASAE*, *35*(5), 1489–1495.

Elliot, W. J. (2004), WEPP internet interfaces for forest erosion prediction, *J. Am. Water Resour. Assoc.*, *40*(2), 299–309, doi:10.1111/j.1752-1688.2004.tb01030.x.

Elliot, W. J., and J. M. Laflen (1993), A process-based rill erosion model, *Trans. ASAE*, *36*(1), 65–72.

Elliot, W. J., A. M. Liebenow, J. M. Laflen, and K. D. Kohl (1989), A compendium of soil erodibility data from WEPP cropland soil field erodibility experiments 1987 & 1988, *Rep. 3*, Natl. Soil Erosion Res. Lab., West Lafayette, Indiana.

Elliot, W. J., L. J. Olivieri, J. M. Laflen, and K. D. Kohl (1990), Predicting soil erodibility from soil strength measurements, presented at the 1990 International Meeting, the American Society of Agricultural Engineers, Columbus, Ohio, 24–27 June.

Ellison, W. D. (1946), Soil detachment and transportation, *Soil Conservation*, *11*(8), 179–190.

Foltz, R. B., H. Rhee, and W. J. Elliot (2008), Modeling changes in rill erodibility and critical shear stress on native surface roads, *Hydrol. Processes*, *22*, 4783–4788, doi:10.1002/hyp.7092.

Foster, G. R. (1982), Modeling the erosion process, in *Hydrologic Modeling of Small Watersheds*, *Am. Soc. Agric. Eng. Monogr.*, vol. 5, edited by C. T. Haan, H. P. Johnson, and D. L. Brakensiek, pp. 297–380, Am. Soc. Agric. Eng., St. Joseph, Mich.

Foster, G. R., and L. D. Meyer (1972), A closed-form soil erosion equation for upland areas, in *Sedimentation: Symposium to Honor Professor H. A. Einstein*, edited by H. W. Shen, pp. 12.1–12.19, Colo. State Univ., Fort Collins.

Foster, G. R., D. C. Flanagan, M. A. Nearing, L. J. Lane, L. M. Risse, and S. C. Finkner (1995), Hillslope erosion component, in *USDA-Water Erosion Prediction Project: Hillslope profile and watershed model documentation*, *Rep. 10*, chap. 11, pp. 11.1–11.12, Natl. Soil Erosion Res. Lab., West Lafayette, Indiana.

Gilley, J. E., and M. A. Weltz (1995), Hydraulics of overland flow, in *USDA-Water Erosion Prediction Project: Hillslope profile and watershed model documentation*, *Rep. 10*, chap. 10, pp. 10.1–10.7, Natl. Soil Erosion Res. Lab., West Lafayette, Indiana.

Giménez, R., and G. Govers (2002), Flow detachment by concentrated flow on smooth and irregular beds, *Soil Sci. Soc. Am. J.*, *66*, 1475–1483.

Govers, G., R. Giménez, and K. Van Oost (2007), Rill erosion: Exploring the relationship between experiments, modelling, and field observations, *Earth Sci. Rev.*, *84*, 87–102, doi:10.1016/j.earscirev.2007.06.001.

Hairsine, P. B., and C. W. Rose (1992a), Modeling water erosion due to overland flow using physical principles: 1. Sheet flow, *Water Resour. Res.*, *28*(1), 237–243, doi:10.1029/91WR02380.

Hairsine, P. B., and C. W. Rose (1992b), Modeling water erosion due to overland flow using physical principles: 2. Rill flow, *Water Resour. Res.*, *28*(1), 245–250, doi:10.1029/91WR02381.

Helsel, D. R., and R. M. Hirsh (2002), Statistical methods in water resources, in *Hydrologic Analysis and Interpretation*, *Tech. Water Resour. Invest. U.S. Geol. Surv., Book 4, Chap. A3*, 1–510.

Knapen, A., J. Poesen, G. Govers, G. Gyssels, and J. Nachtergaele (2007), Resistance of soils to concentrated flow erosion: A review, *Earth Sci. Rev.*, *80*, 75–109, doi:10.1016/j.earscirev.2006.08.001.

Laflen, J. M., W. J. Elliot, J. R. Simanton, C. S. Holzhey, and K. D. Kohl (1991), WEPP soil erodibility experiments for rangeland and cropland soils, *J. Soil Water Conserv.*, *46*, 39–44.

Laflen, J. M., W. J. Elliot, D. C. Flanagan, C. R. Meyer, and M. A. Nearing (1997), WEPP—Predicting water erosion using a process-based model, *J. Soil Water Conserv.*, *52*(2), 96–102.

Littel, R. C., G. A. Milliken, W. W. Stroup, R. D. Wolfinger, and O. Schabenberger (2006), *SAS® for Mixed Models*, 2nd ed., SAS Inst., Cary, N. C.

McIsaac, G. F., J. K. Mitchell, J. W. Hummel, and W. J. Elliot (1992), An evaluation of unit stream power theory for estimating soil detachment and sediment discharge from tilled soils, *Trans. ASAE*, *35*(2), 535–544.

Moffet, C. A., F. B. Pierson, P. R. Robichaud, K. E. Spaeth, and S. P. Hardegree (2007), Modeling soil erosion on steep sagebrush rangeland before and after prescribed fire, *Catena*, *71*, 218–228, doi:10.1016/j.catena.2007.03.008.

Morgan, R. P. C., J. N. Quinto, R. E. Smith, G. Govers, J. W. A. Poesen, K. Auerswald, G. Chisci, D. Torri, and M. E. Styczen (1998), The European soil erosion model (EUROSEM): A dynamic approach for predicting sediment transport from fields and small catchments, *Earth Surf. Processes Landforms*, *23*, 527–544, doi:10.1002/(SICI)1096-9837(199806)23:6<527::AID-ESP868>3.0.CO;2-5.

Nearing, M., G. Foster, L. Lane, and S. Finkner (1989), A process-based soil erosion model for USDA-Water Erosion Prediction Project technology, *Trans. ASAE*, *32*(5), 1587–1593.

Nearing, M., L. Norton, D. Bulgakove, G. Larionov, L. West, and K. Dontsova (1997), Hydraulics and erosion in eroding rills, *Water Resour. Res.*, *33*(4), 865–876, doi:10.1029/97WR00013.

Nearing, M. A., J. R. Simanton, L. D. Norton, S. J. Bulygin, and J. Stone (1999), Soil erosion by surface water flow on a stony, semiarid hillslope, *Earth Surf. Processes Landforms*, *24*, 677–686, doi:10.1002/(SICI)1096-9837(199908)24:8<677::AID-ESP981>3.0.CO;2-1.

Ott, L. (1993), *An Introduction to Statistical Methods and Data Analysis*, 4th ed., Wadsworth, Belmont, Calif.

Pannkuk, C. D., and P. R. Robichaud (2003), Effectiveness of needle cast at reducing erosion after forest fires, *Water Resour. Res.*, *39*(12), 1333, doi:10.1029/2003WR002318.

Pierson, F. B., P. R. Robichaud, C. A. Moffet, K. E. Spaeth, S. P. Hardegree, P. E. Clark, and C. J. Williams (2008), Fire effects on rangeland hydrology and erosion in a steep sagebrush-dominated landscape, *Hydrol. Processes*, *22*, 2916–2929, doi:10.1002/hyp.6904.

Robichaud, P. R. (1996), Spacially varied erosion potential from harvested hillslopes after prescribed fire in the interior Northwest, Ph.D. thesis, Univ. of Idaho, Moscow.

Robichaud, P. R. (2000), Fire effects on infiltration rates after prescribed fire in northern Rocky Mountain forests, USA, *J. Hydrol.*, *231–232*, 220–229, doi:10.1016/S0022-1694(00)00196-7.

Robichaud, P. R., J. W. Wagenbrenner, and R. E. Brown (2010), Rill erosion in natural and disturbed forests: 1. Measurements, *Water Resour. Res.*, *46*, W10506, doi:10.1029/2009WR008314.

SAS Institute (2008), *SAS® for Windows 9.2*, SAS Inst., Cary, N. C.

Sheridan, G. J., P. N. J. Lane, and P. J. Noske (2007), Quantification of hillslope runoff and erosion processes before and after wildfire in a wet Eucalyptus forest, *J. Hydrol.*, *343*, 12–28, doi:10.1016/j.jhydrol.2007.06.005.

Yalin, M. S. (1963), An expression for bed-load transport, *J. Hydraul. Div. Am. Soc. Civ. Eng.*, *89*, 221–250.

W. J. Elliot, P. R. Robichaud, and J. W. Wagenbrenner, Forestry Sciences Laboratory, Rocky Mountain Research Station, Forest Service, U.S. Department of Agriculture, 1221 South Main St., Moscow, ID 83843, USA. (probichaud@fs.fed.us)